Surface and magnetic polaritons on two-dimensional nanoslab-aligned multilayer structure

Zhijian Zhang,[1] Keunhan Park,[2] and Bong Jae Lee[3,*]

[1]*Department of Mechanical Engineering and Material Science, University of Pittsburgh, Pittsburgh, Pennsylvania 15261, USA*
[2]*Department of Mechanical, Industrial and Systems Engineering, University of Rhode Island, Kingston, Rhode Island 02881, USA*
[3] *Department of Mechanical Engineering, Korea Advanced Institute of Science and Technology, Daejeon 305-701, South Korea*
[*]*bongjae.lee@kaist.ac.kr*

Abstract: The present study theoretically investigates the radiative properties of a two-dimensional (2-D) multilayer structure that has a dielectric spacer between a metallic substrate and square cross-sectional metallic gratings. Differently from the one-dimensional metallic strips coated on a dielectric spacer atop an opaque metallic film [Opt. Express **16**, 11328 (2008)], the 2-D metallic gratings can support the localized surface plasmon in addition to the propagating surface plasmon along the metal-dielectric interface. Moreover, the presence of a dielectric spacer also allows the excitation of magnetic polaritons. Underlying mechanisms of the surface and magnetic polartions on the proposed structure are elucidated by employing the 2-D rigorous coupled-wave analysis. The results obtained in this study will advance our fundamental understanding of light-matter interaction at the nanometer scale and will facilitate the development of engineered nanostructures for real-world applications, such as thermophotovoltaic and photovoltaic devices.

OCIS codes: (160.4760) Optical properties; (240.5420) Polaritons.

References and links

1. J. N. Anker, W. P. Hall, O. Lyandres, N. C. Shah, J. Zhao, and R. P. Van Duyne, "Biosensing with plasmonic nanosensors," Nat. Mater. **7**, 442–453 (2008).
2. S. Pillai, K. R. Catchpole, T. Trupke, and M. A. Green, "Surface plasmon enhanced silicon solar cells," J. Appl. Phys. **101**, 093105 (2007).
3. W. Srituravanich, N. Fang, C. Sun, Q. Luo, and X. Zhang, "Plasmonic nanolithography," Nano Lett. **4**(6), 1085–1088 (2004).
4. I. R. Hooper and J. R. Sambles "Surface plasmon polaritons on thin-slab metal gratings," Phys. Rev. B **67**, 235404 (2003).
5. H. F. Ghaemi, T. Thio, and D. E. Grupp, "Surface plasmons enhance optical transmission through subwavelength holes," Phys. Rev. B **58**, 6779–6782(1998).
6. T. Thio, K. M. Pellerin, R. A. Linke, H. J. Lezec, and T. W. Ebbesen, "Enhanced light transmission through a single subwavelength aperture," Opt. Lett. **26**(24), 1972–1974 (2001).
7. C. Zhao and J. Zhang, "Binary plasmonics: launching surface plasmon polaritons to a desired pattern," Opt. Lett. **34**(16), 2417–2419 (2009).
8. S. Chang and S. K. Gray, "Surface plasmon generation and light transmission by isolated nanoholes and arrays of nanoholes in thin metal films," Opt. Express **13**(8), 3150-3165 (2008).

#149604 - $15.00 USD Received 21 Jun 2011; revised 30 Jul 2011; accepted 3 Aug 2011; published 10 Aug 2011

9. J. W. Lee, M. A. Seo, D. H. Kang, K. S. Khim, S. C. Jeoung, and D. S. Kim, "Terahertz electromagnetic wave transmission through random arrays of single rectangular holes and slits in thin metallic sheets," Phys. Rev. Lett. **99**, 137401 (2007).
10. M. A. Seo, A. J. L. Adam, J. H. Kang, J. W. Lee, K. J. Ahn, Q. H. Park, P. C. M. Planken, and D. S. Kim, "Near field imaging of terahertz focusing onto rectangular apertures," Opt. Express **16**(23), 20484–20489 (2008).
11. M. Yamamoto, K. Araya, and F. J. Garcia de Abajo, "Photon emission from silver particles induced by a high-energy electron beam," Phys. Rev. B **64**, 205419 (2001).
12. A. J. Haes and R. P. Van Duyne, "A nanoscale optical biosensor: sensitivity and selectivity of an approach based on the localized surface plasmon resonance spectroscopy of triangular silver nanoparticles," J. Am. Chem. Soc. **124**(35), 10596–10640 (2002).
13. J. M. Pitark, V. M. Silkin, E. V. Chulkov, and P. M. Echenique, "Theory of surface plasmons and surface-plasmon polaritons," Rep. Prog. Phys. **70**, 1–87 (2007).
14. H. Raether, *Surface Plasmons on Smooth and Rough Surfaces and on Gratings* (Springer-Verlag, 1988).
15. A. K. Sarychev, G. Shvets, and V. M. Shalaev, "Magnetic polariton resonance," Phys. Rev. E **73**, 036609 (2006).
16. J. B. Pendry, A. J. Holden, D. J. Robbins, and W. J. Stewart, "Magnetism from conductors and enhanced nonlinear phenomena," IEEE Trans. Microwave Theory Tech. **47**, 2075–2084 (1999).
17. S. Linden, C. Enkrich, M. Wegener, J. F. Zhou, T. Koschny, and C. M. Soukoulis, "Magnetic response of metamaterials at 100 Terahertz," Science **306**, 1351–1353 (2004).
18. C. Enkrich, M. Wegener, S. Linden, S. Burger, L. Zschiedrich, F. Schmidt, J.F. Zhou, T. Koschny, and C. M. Soukoulis, "Magnetic metamaterials at telecommunication and visible frequencies," Phys. Rev. Lett. **95**, 203901 (2005).
19. J. F. Zhou, E. N. Economon, T. Koschny, and C. M. Soukoulis, "Unifying approach to left-handed material design," Opt. Lett. **31**(24), 3620–3622 (2006).
20. M. Kafesaki, I. Tsiapa, N. Katsarakis, T. Koschny, C. M. Soukoulis, and E. N. Economou, "Left-handed metamaterials: the fishnet structure and its variations," Phys. Rev. B **75**, 2345114 (2007).
21. J. Valentine, S. Zhang, T. Zentgraf, E. Ulin-Avila, D. A. Genov, G. Bartal, and X. Zhang, "Three-dimensional optical metamaterial with a negative refractive index," Nature **455**, 376–379 (2008).
22. B. J. Lee, L. P. Wang, and Z. M. Zhang, "Coherent thermal emission by excitation of magnetic polaritons between periodic strips and a metallic film," Opt. Express **16**(15), 11328–11336 (2008).
23. W. Cai and V. Shalaev, *Optical Metamaterials: Fundamentals and Applications* (Springer, 2009).
24. E. D. Palik, *Handbook of Optical Constants of Solids* (Academic Press, 1998).
25. B. J. Lee, Y.-B. Chen, and Z. M. Zhang, "Confinement of infrared radiation to nanometer scales through metallic slit arrays," J. Quant. Spectrosc. Radiat. Trans. **109**, 608–619 (2008).
26. B. J. Lee, Y.-B. Chen, and Z.M. Zhang, "Transmission enhancement through nanoscale metallic slit arrays from the visible to mid-infrared," J. Comput. Theor. Nanosci. **5**(2), 201–213 (2008).
27. M. G. Moharam and T. K. Gaylord, "Rigorous coupled-wave analysis of planar-grating diffraction," J. Opt. Soc. Am. **71**(7), 811–818 (1981).
28. M. G. Moharam and T. K. Gaylord, "Rigorous coupled-wave analysis of metallic surface-relief gratings," J. Opt. Soc. Am. A **3**(11), 1780–1789 (1986).
29. Y.-B. Chen and K.-H. Tan, "The profile optimization of periodic nano-structure for wavelength-selective thermophotovoltaic emitters," Int. J. Heat Mass Transfer **53**, 5542–5551 (2010).
30. J. Jiang, *Rigorous Analysis and Design of Diffractive Optical Elements* (Ph. D. Dissertation, The University of Alabama in Huntsville, 2000).
31. J. D. Jackson, *Classical Electrodynamics* (John Wiley & Sons, 1999).
32. V. A. Podolskiy, A. K. Sarychev, and V. M. Shalaev, "Plasmon modes in metal nanowires and left-handed materials," J. Nonlinear Opt. Phys. Mater. **11**, 65–74 (2002).
33. K. Park, B. J Lee, C. Fu, and Z. M. Zhang, "Study of the surface and bulk polaritons with a negative index metamaterial," J. Opt. Soc. Am. B **22**(5), 1016–1023 (2005).
34. C. F. Bohren and D. R. Huffman, *Absorption and Scattering of Light by Small Particles* (Wiley-VCH, 1998).
35. E. Hutter and J. H. Fendler, "Exploitation of Localized Surface Plasmon Resonance," Adv. Mat. **16**(19), 1685–1706 (2004).
36. M. A. El-Sayed,"Some interesting properties of metals confined in time and nanometer space of different shapes," Acc. Chem. Res. **34**(4), 257–264 (2001).

1. Introduction

Tailoring the radiative properties, such as reflectance, transmittance, and absorptance, with engineered nanostructures has recently drawn much attention due to their great potential in many promising applications, such as biosensing [1], thermophotovoltaic and photovoltaic energy conversions [2], and nano-manufacturing [3]. The spectral- and/or directional-selectivity in the

#149604 - $15.00 USD Received 21 Jun 2011; revised 30 Jul 2011; accepted 3 Aug 2011; published 10 Aug 2011

radiative properties of engineered nanostructures often result from the excitation of resonance phenomena, such as surface plasmon polariton (SPP). Note that SPPs can be observed in periodic metallic structures, such as one-dimensional (1-D) gratings [4], two-dimensional (2-D) hole arrays [5], bulls eye structure [6], and binary plasmonic structure [7], where the reciprocal lattice vector of the periodic structure compensates the momentum difference between the surface plasmon and the incident light. One the other hand, the localized surface plasmon (LSP) has been found on the isolated subwavelength structure, such as a single hole on a thin metal film [8–10] and nanoparticles [11, 12]. The key underlying mechanism of the SPP and LSP is the coupling of the incident wave with the collective charge density oscillations on the conductor [13]; hence they are usually observed at the metal-dielectric interface. Since the energy and momentum of the incident light have to match with those of the SPP, the SPP resonance usually depends on the frequency and the incidence angle of the incident wave [14].

In addition to SPPs, the magnetic resonance (or magnetic polariton) has been extensively studied since it can induce the coupling between the magnetic-field component of the incident wave and the matter, allowing one to tailor the optical properties of materials in an unprecedented manner [15]. For instance, Pendry first proposed to use a split-ring resonator to achieve the effective negative permeability resulting from the diamagnetism [16]. Afterwards, the single split-ring [17] and U-shape cells [18] have been demonstrated as the magnetic resonators. The magnetic resonance also occurs with paired metal strips when the anti-parallel currents flow in different metallic layers [19]. The magnetic resonance observed in the double-layered or multilayered fishnet structure [20, 21] is discovered to be a very good candidate for achieving bulk negative-index materials. The magnetic resonance has also been employed to control the thermal emission characteristics. For instance, Lee *et al*. [22] recently found that the 1-D metallic grating coated on a dielectric spacer atop an opaque metal substrate can enhance the performance of thermal emitter or thermal collector by exciting the magnetic polariton (MP). Distinctly from the SPP and the LSP, the key underlying mechanism of the MP is the coupling of the incident wave with the anti-parallel current on the metallic strips separated by a dielectric spacer [15, 23].

Although a number of studies have designed nanostructures to control the radiative properties using the SPP, LSP and the MP, most of them have mainly relied on 1-D structures due to the simplicity in modeling and often attempted to extrapolate the 1-D results to the 2-D structures. However, there is no theoretical evidence that radiative properties of 1-D structures can be extrapolated to 2-D with the same resonance features when the identical geometries are used in 2-D structures. Since real-world applications tailoring the radiative properties more likely have 2-D nanostructures than 1-D due to the reality of manufacturing, it is imperative to investigate the tailoring of the radiative properties with the polariton phenomena in 2-D nanostructures. Moreover, using 2-D structures will overcome the current challenge of 1-D structures that control the radiative properties only in a specific direction and polarization state. Inspired by the previous work done on the 1-D structure [22], the present work aims to theoretically investigate the radiative properties of 2-D metallic grating structures that have square and rectangular nanoslabs periodically patterned on top of a dielectric-layered metallic substrate. The 2-D rigorous coupled-wave analysis (RCWA) was developed in order to compute the radiative properties of 2-D nanostructures as well as the magnetic field distribution in the near field. In the following sections, the theoretical modeling will be briefly discussed, and different resonance modes, i.e., SPP, LSP and MP modes, excited on the proposed structure and their underlying mechanisms will be elucidated. The interactions between SPP, LSP, and MP modes will also be investigated to seek out the feasibility in achieving the enhanced absorption at the broad spectral range with the quasi-isotropic manner. The present work will clearly address the difference of the surface and magnetic polartions on the 2-D structure from those on the 1-D structure, which

#149604 - $15.00 USD Received 21 Jun 2011; revised 30 Jul 2011; accepted 3 Aug 2011; published 10 Aug 2011

will eventually help to design optimal nanostructures for thermophotovoltaic or photovoltaic applications.

2. Theoretical Modeling

Figure 1 depicts one unit cell of the 2-D nanoslab-aligned grating structure, where square slabs are aligned in forming the 2-D square lattice on the top of the dielectric-layered Ag substrate. The following geometric parameters were chosen by optimizing the frequency as well as the value of the reflectance dip. The period Λ for the grating is 500 nm for both the x-direction and the y-direction. The nanoslab is squared with width $w = 250$ nm and its thickness d_g is 30 nm. The thickness of the SiO_2 film d_f is 25 nm. In general, w and d_f affect the resonance frequency of the magnetic polariton, Λ affects the resonance frequency of the surface plasmon, and d_g affects the reflectance dip value. Note that the Ag substrate can be regarded as opaque since its thickness is much larger than the radiation penetration depth; thus, small reflectance dip value means the large absorption of the incident radiation. In the present study, the optical properties of Ag and SiO_2 are obtained from Ref. [24]. A linearly polarized electromagnetic wave is incident from air at the incidence angle θ_x. Because of the symmetry, we only consider that the incident angle is rotated in the x-z plane. In addition, p-polarization is defined as the case in which the magnetic field is parallel with y-direction as shown in Fig. 1 and s-polarization as the electric field parallel with y-direction.

In order to accurately predict the radiative properties of the proposed 2-D grating structure, the present work developed the 2-D RCWA algorithm that solves Maxwell's equations for the electromagnetic wave diffracted by the periodic structures (or gratings). In the RCWA algorithm, the electric and magnetic fields in the incident, grating, and transmitted media are expanded as a summation of multiple diffraction orders. Due to the periodicity of the grating structure, the dielectric function (or relative electric permittivity) of the grating region can be expressed as a Fourier expansion. By matching the boundary conditions (i.e., continuity of tangential components of electric and magnetic fields) at boundaries of the incident, grat-

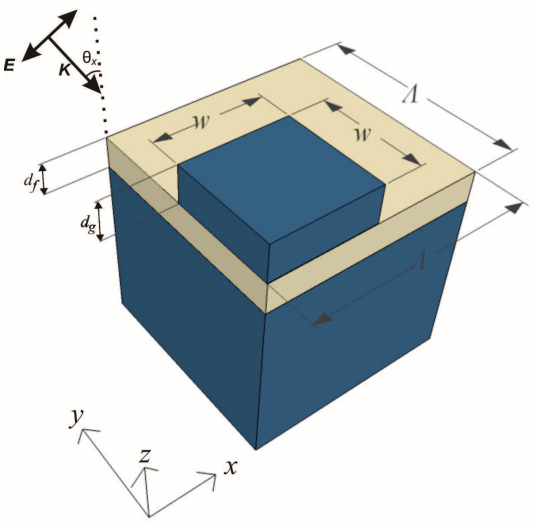

Fig. 1. Schematic of one unit cell of the 2-D nanoslab-aligned multilayer structure. The geometric parameters are the grating period $\Lambda = 500$ nm, the dielectric film thickness $d_f = 25$ nm, the grating (or slab) thickness $d_g = 30$ nm, and the slab width $w = 250$ nm.

#149604 - $15.00 USD Received 21 Jun 2011; revised 30 Jul 2011; accepted 3 Aug 2011; published 10 Aug 2011

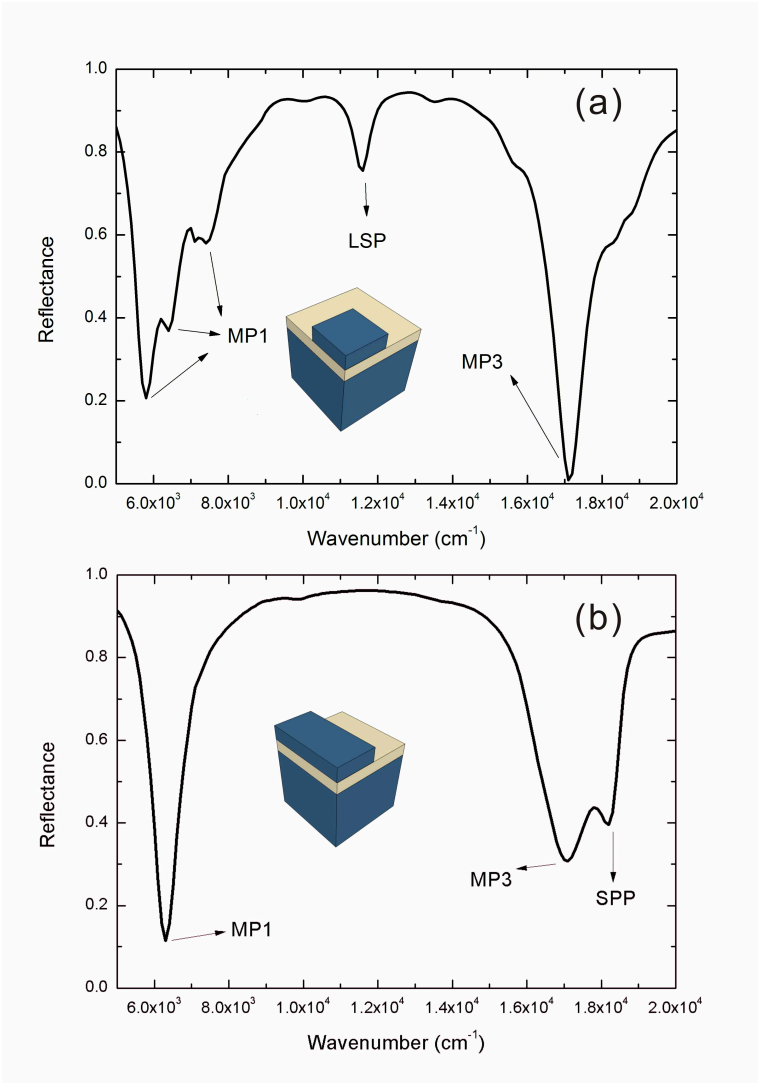

Fig. 2. Reflectance spectrum at normal incidence for *p*-polarization: (a) 2-D nanoslab-aligned multilayer structure; and (b) 1-D strip-aligned multilayer structure.

ing, and transmitted media, closed linear equations can be obtained. The RCWA algorithm is widely used in near-field optics and plasmonics because of its good convergence and accuracy, especially when the grating period is comparable with the wavelength of the incident light [25, 26]. The accuracy of the solution provided by RCWA solely depends on the order of the space-harmonic expansion of the field. Therefore it is easy to balance the computation time and accuracy. Although the RCWA for the 1-D structure is well developed [27, 28], the 2-D RCWA is still under investigation because of the complexity in the formulations especially for the multilayer structures [29, 30]. In this paper, we extended the 1-D RCWA code [26] to the 2-D situation and applied it for 2-D multilayer grating structures. Detailed mathematical formulations for the 2-D RCWA can be found in elsewhere [30]; hence equations are not provided here.

#149604 - $15.00 USD Received 21 Jun 2011; revised 30 Jul 2011; accepted 3 Aug 2011; published 10 Aug 2011

Figure 2(a) shows the normal reflectance calculated using the 2-D RCWA in the wavenumber range from 5000 to 20000 cm^{-1}. For comparison, the *p*-polarized, normal reflectance of the 1-D strip-aligned multilayered grating structure is plotted in Fig. 2(b). This 1-D multilayered grating structure has the identical geometry with the 2-D structures except being 1-D, i.e., $\Lambda = 500$ nm, $d_f = 25$ nm, $d_g = 30$ nm, and $w = 250$ nm. In order to verify the accuracy of our 2-D RCWA code (with ± 18 diffraction orders into both *x*- and *y*-directions), we compared the result shown in Fig. 2(b), which was calculated using the 2-D RCWA, with the 1-D RCWA method with ± 40 diffraction orders on the same structure. The difference between 1-D and 2-D RCWA calculations is less than 0.3%, verifying the developed 2-D RCWA.

It is interesting to see that Fig. 2(b) has three fundamental modes of MP (indicated as MP1) at 5800, 6400 and 7400 cm^{-1}. The 2D structure also supports the LSP at 11600 cm^{-1}, where the nanoslab stands as an isolated subwavelength object. For the 1-D structure, although the metal strip can also be considered as a subwavelength object like nano-ribbon, the LSP is not observed in the considered wavenumber range. This may be because metal strips do not act like an isolated nanostructure but act like a periodic array in the considered wavenumber range, such that diffraction is dominant over the scattering. The dip around 17200 cm^{-1} is the third-order harmonic mode of MP (indicated as MP3) coupled with the SPP mode, and will be discussed in more details in the consecutive section. The MP modes are also excited in the 1-D structure, as shown in Fig. 2(b). However, each MP mode has only one branch, and the MP3 mode is slightly separated from the SPP due to the interactions of both modes. For the *s*-polarized incidence, the 1-D structure does not support any resonance mode, and 2-D structures exhibits the identical reflectance spectrum as *p*-polarization due to the symmetry of the square nano slab.

3. Magnetic Polariton Modes

Magnetic polariton by definition is the resonance of magnetic oscillation on material surface coupled with incident light, which depends mostly on the plasmonic properties and geometry of the material [23]. Key parameters for the light-matter interaction are the electric permittivity and the magnetic permeability. The magnetic permeability is the amplitude of magnetization that a material obtains in response to the incident electromagnetic wave [31]. In nature, the real part of the magnetic permeability is positive, indicating that the total magnetic field decreases in the material. However, when magnetic polaritons are excited, the material response resonantly enhances the total magnetic field due to the occurrence of strong diamagnetism, altering the real part of the magnetic permeability to be negative. The strong resonance of total magnetic field of the material can be manifested as enhanced absorption for the opaque structure [22]. For the nanoslab-aligned multilayer structure shown in Fig. 1, the occurrence of diamagnetism can be explained as follows [32]: the incident light produces oscillating magnetic field, which in turn induces a current in the nanoslab along one direction and another current near the surface of the metal substrate in the opposite direction. These anti-parallel currents induce the diamagnetic response, which excites the magnetic polariton.

In order to investigate the MP modes in more details, we calculated the reflectance of the nanoslab-aligned multilayer structure at *p*-polarization with different incidence angles, as shown in Fig. 3. The fundamental magnetic polariton (MP1) mode for the 2-D nanoslab-aligned structure turns out to be split into multiple branches at 5800 (MP1a), 6400 (MP1b) and 7400 cm^{-1} (MP1c), and they barely change for different incidence angles. In order to verify that these branches correspond to the MP1 mode, Fig. 4 plots the magnetic field distributions for those three dips at the interface between the SiO_2 film and the Ag substrate (refer to Fig. 4(a)) for the normal incidence (i.e., $\theta_x = 0^\circ$). The magnetic field shown in Fig. 4 is normalized with the incident magnetic field. Because of the diamagnetic response accompanied with the MP, the magnetic field should be strongly confined in the dielectric region sandwiched by

#149604 - $15.00 USD Received 21 Jun 2011; revised 30 Jul 2011; accepted 3 Aug 2011; published 10 Aug 2011

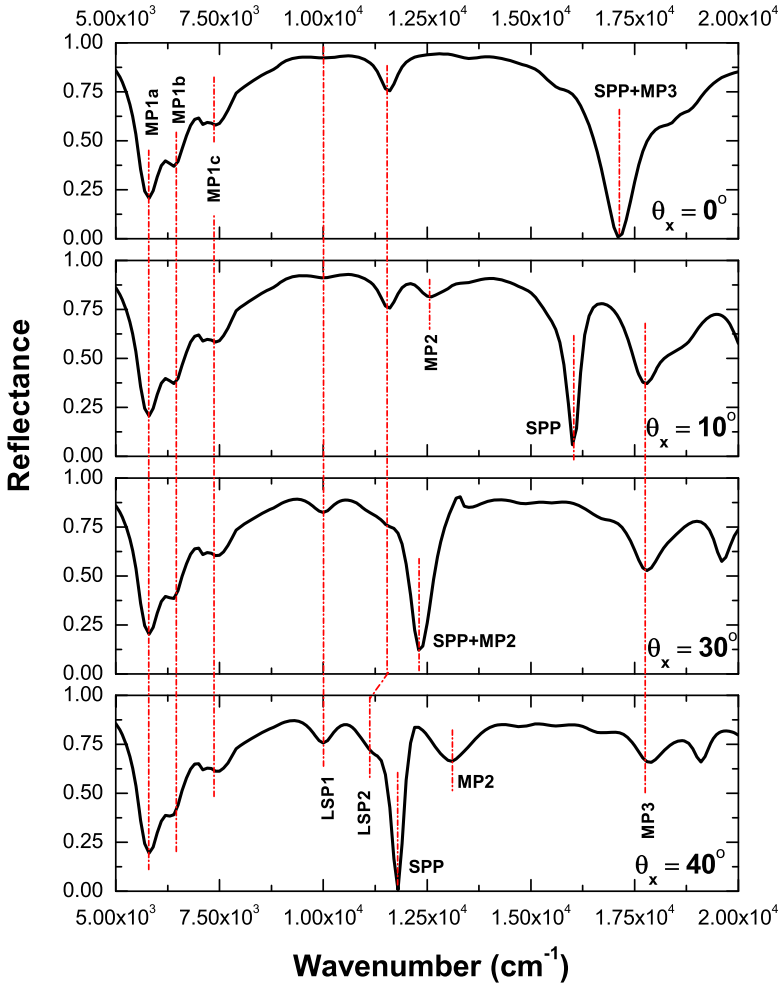

Fig. 3. Reflectance spectra of the nanoslab-aligned multilayer structure for different θ_x values. The incident light is *p*-polarized.

the nanoslab and the substrate. As can be seen from Figs. 4(b), 4(c), and 4(d), all branches have only one, strongly localized resonance loop of the magnetic field in the nanoslab, indicating that all the dips belong to the fundamental mode. The exact physical mechanism for the splitting of the MP1 mode is still unclear, which need further investigation in the future. One possible mechanism may be explained from the localization of the magnetic field both into *x*- and *y*-directions. In addition to the magnetic-field localization in the *x*-direction, as is the case of the 1-D structure, additional *y*-directional confinement of the magnetic field may introduce multiple branches of the MP1 modes.

The enhancement factor of the magnetic-field localization for MP1 modes is on the order of ten. When comparing Fig. 3 and Fig. 4, it is interesting to note that while the MP1a provides the smallest reflectance, the maximum enhancement of the magnetic field occurs at MP1b.

#149604 - $15.00 USD Received 21 Jun 2011; revised 30 Jul 2011; accepted 3 Aug 2011; published 10 Aug 2011

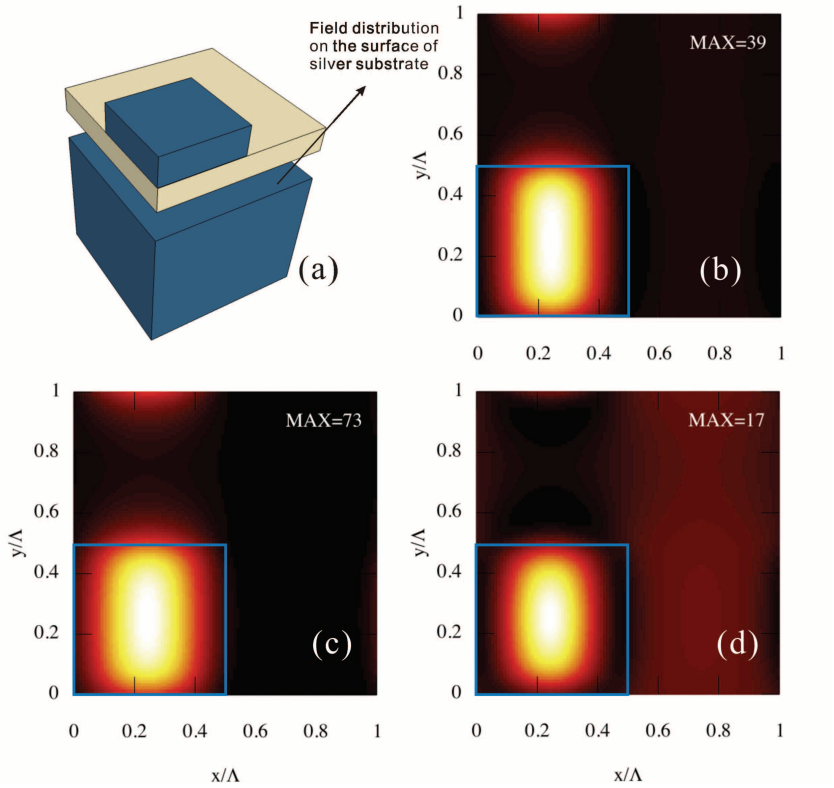

Fig. 4. (a) Schematic of the plane where the magnetic field is calculated and plotted. The magnetic field distribution for the reflectance dips at: (b) 5800 cm^{-1}; (c) 6400 cm^{-1}; and (d) 7400 cm^{-1} for normal incidence. The magnetic field is normalized by the incidence magnetic field as $|H_y|^2/|H_{y,inc}|^2$. The brighter color implies the stronger field and "MAX" stands for the maximum value of $|H_y|^2/|H_{y,inc}|^2$ in the plane. The blue square indicates the position of the nanoslab.

This strongly suggests that the reflectance dip value is not directly related to the strength of the magnetic polariton. In fact, it is technically difficult to inversely trace all the resonance modes from the reflectance spectrum. For example, even in a simple attenuated total reflection configuration, some of the plasmonic modes cannot be found from the reflectance dips [33].

Besides the fundamental mode, the third order harmonic mode (MP3) is also excited at around 17800 cm^{-1}, as shown in Fig. 3. Figure 5(a) shows the normalized magnetic field on the interface between the SiO_2 film and the silver substrate when the MP3 mode is excited at 17800 cm^{-1} for $\theta_x = 10°$. The magnetic field distribution clearly shows three anti-nodes along the *x*-direction under the nanoslab space, verifying that this reflectance dip is caused by the MP3 mode. It should be noted that the MP3 mode is also excited for the normal incidence. However, for the geometry investigated in the present paper the MP3 mode at the normal incidence is coupled with the SPP to make almost zero reflectance value at 17100 cm^{-1}. Further details of the MP-SPP coupling will be discussed in the consecutive section. The second-order harmonic mode (MP2) can also be excited by the same structure under consideration, but only at oblique incidence angles. The MP2 mode cannot be excited at the normal incidence because two anti-parallel current loops formed at the MP2 mode are mirror-symmetric for the normal incidence and thus will cancel the induced magnetic moments [22]. Figure 3 shows the re-

#149604 - $15.00 USD Received 21 Jun 2011; revised 30 Jul 2011; accepted 3 Aug 2011; published 10 Aug 2011

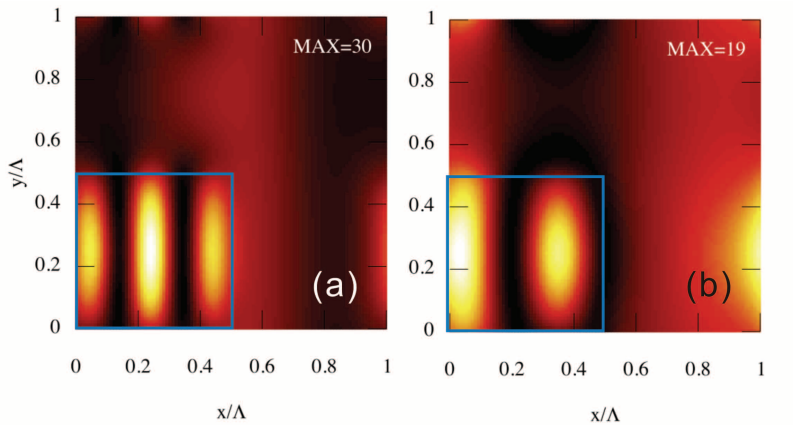

Fig. 5. The magnetic field distribution at the interface between the SiO_2 film and the Ag substrate at: (a) 17800 cm^{-1} for $\theta_x = 10°$; and (b) 12600 cm^{-1} for $\theta_x = 10°$.

flectance dip caused by the MP2 mode for different incidence angles, i.e., at 12600 cm^{-1} for $\theta_x = 10°$, at 12300 cm^{-1} for $\theta_x = 30°$ and at 13100 cm^{-1} for $\theta_x = 40°$. According to the equivalent inductor-capacitor (LC) circuit model [19, 23], the MP2 mode should occur at the same frequency for different incidence angles. The slight variations in the resonance frequency of the MP2 mode for different incidence angles may be due to the interaction with the SPP and LSP. The normalized magnetic field at 12600 cm^{-1} and $\theta_x = 10°$ shown in Fig. 5(b) exhibits two anti-nodes in the nanoslab-covered space, demonstrating the excitation of the MP2 mode.

The equivalent LC circuit model predicted that for the 1-D multilayered grating structure the resonance frequency of the MP mainly depends on the local geometry of the nanostructure (i.e., d_f and w) and the optical properties of materials, but not on the unit cell period Λ and the incidence angle θ_x [22]. This claim remains valid for the 2-D structure, as shown in Figs. 3 and 6. Figure 6 shows the reflectance spectrum for *s*-polarization at the same incidence angles as Fig. 3. Regardless of the polarization states, MP1 occurs at 5800, 6400 and 7400 cm^{-1}, and MP3 occurs in the region of 17100 $\sim$ 17900 cm^{-1}. Again, the MP-SPP coupling causes the slight shift of the reflectance dip locations as the incidence angle varies. Although not shown in this paper, the magnetic field distributions on the SiO_2 layer/Ag substrate interface were also calculated at each reflectance dip for *s*-polarization: they look almost the same as Figs. 4 and 5 except that the direction of anti-nodes is in the *y*-direction. One big difference between *p*- and *s*-polarizations is that the *s*-polarized light cannot excite the MP2 mode even if θ_x varies. For *s*-polarization, two current loops with opposite direction should be formed along the *y*-direction when the MP2 mode condition is satisfied. However, varying θ_x does not break the symmetry of those current loops. Therefore, the resulting averaged magnetic moment is always zero regardless of θ_x for *s*-polarization.

4. Surface Plasmon Polariton Modes

4.1. Surface Plasmon and its Coupling with the Magnetic Polariton

A surface plasmon is a collective excitation of electrons at the interface between a dielectric and a conductor [14]. Because of the non-radiative nature of the surface plasmon polariton, the parallel component of the SPP wavevector is always larger than the free space wavevector, requiring a coupler to excite the SPP with a propagating wave. When the light is incident on the 2-D nanoslab-aligned multilayer structure, periodic nanoslabs diffract the light into different

#149604 - $15.00 USD Received 21 Jun 2011; revised 30 Jul 2011; accepted 3 Aug 2011; published 10 Aug 2011

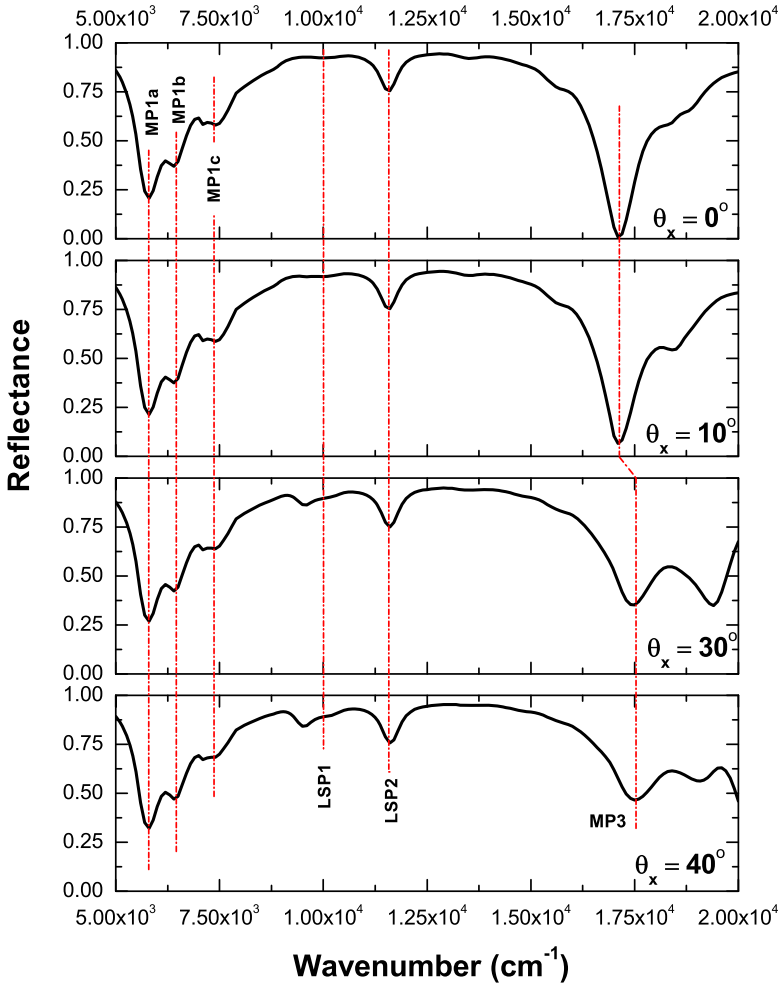

Fig. 6. Reflectance spectra of the nanoslab-aligned multilayer structure for different θ_x values. The incident light is *s*-polarized.

orders, such that the parallel wavevector component of each diffracted light is modified by the reciprocal lattice vector of the periodic structure. Therefore, the SPP will be excited at the interface between the SiO_2 layer and the Ag substrate when the SPP wavevector $\mathbf{k}_{spp}$ matches with one of parallel wavevector components of the diffracted waves, as noted by

$$\mathbf{k}_{spp} = \mathbf{k}_{\parallel,inc} + \frac{2\pi i}{\Lambda}\hat{\mathbf{x}} + \frac{2\pi j}{\Lambda}\hat{\mathbf{y}} \tag{1}$$

where $\mathbf{k}_{\parallel,inc}$ is the parallel component of the incident wavevector, i and j are the diffraction orders into the x- and y-direction, respectively, and $\hat{\mathbf{x}}$ and $\hat{\mathbf{y}}$ are the unit direction vectors into the x- and y-direction. The above equation suggests that the SPP resonance condition is sensitive to the incidence angle and the grating period, but independent of w and d_g. Based on Eq. (1), the

#149604 - $15.00 USD Received 21 Jun 2011; revised 30 Jul 2011; accepted 3 Aug 2011; published 10 Aug 2011

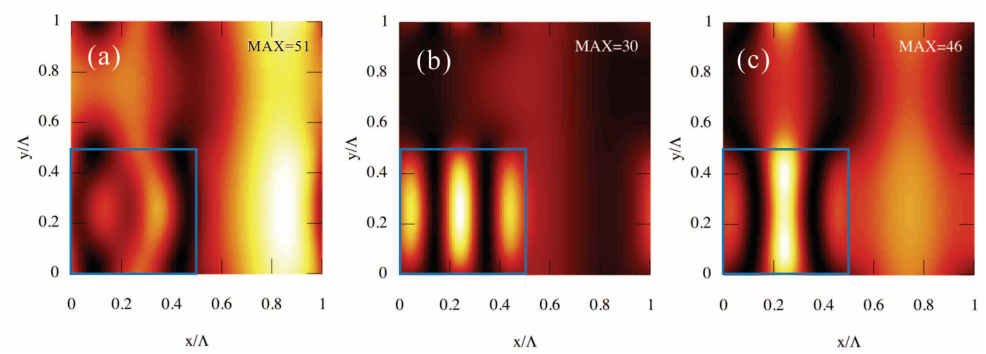

Fig. 7. The magnetic field distribution at the interface between the SiO_2 film and the Ag substrate at: (a) 16000 cm^{-1} for $\theta_x = 10°$; (b) 17800 cm^{-1} for $\theta_x = 10°$; and (c) 17100 cm^{-1} for normal incidence.

(1,0) SPP mode (i.e., $i = 1$, $j = 0$) for the normal incidence is predicted to occur at 18200 cm^{-1}. This prediction is slightly offset from the reflectance dip at 17100 cm^{-1} for $\theta_x = 0°$ in Fig. 3. We believe that this deviation is due to the coupling between the SPP and the MP3 mode. As observed from the oblique incidence angles in Fig. 3, the MP3 mode is supposed to be excited at 17600 cm^{-1}, but is coupled with the SPP excitation to have the reflectance dip at 17100 cm^{-1} instead upon the normal incidence. When the incidence angle changes to $\theta_x = 10°$, the SPP and MP3 modes are decoupled to show two separate dips, SPP at 16000 cm^{-1} and MP3 at 17600 cm^{-1}, respectively. However, it is worthwhile to note that the reflectance dip due to the coupling of the SPP and MP3 is deeper than the pure SPP or MP3 mode.

In order to further elucidate the coupling of the SPP with the MP3 mode, Fig. 7 presents the normalized magnetic field at the interface between SiO_2 film and the Ag substrate for three cases: (1) pure SPP mode at 16000 cm^{-1} for $\theta_x = 10°$, see Fig. 7(a); (2) pure MP3 modes at 17800 cm^{-1} for $\theta_x = 10°$, see Fig. 7(b); and (3) SPP-MP3 coupled mode at 17100 cm^{-1} for the normal incidence, see Fig. 7(c). As expected, Fig. 7(a) demonstrates the propagating nature of the SPP along the surface, such that the enhanced field is distributed over the entire unit cell. This is because the SPP is only localized in the *z*-direction while propagating on the *x*-*y* plane. On the other hand, the field distribution for the MP3 mode clearly exhibits the strong localization on the nanoslab-covered surface with three anti-node formation. The field distribution for the coupled SPP and MP3 mode shows combined characteristics of the SPP and MP3 modes.

It should be noted that the SPP can also be coupled with the MP2 modes, as shown in Fig. 3 for $\theta_x = 30°$. However, the interaction of surface plasmons with magnetic polaritons exhibits different characteristics depending on the harmonic order of the magnetic resonance, as indicated in Fig. 2(b) of Ref. [22]. It was found that when the SPP interacts with the MP2, the anti-crossing effect occurs to split the MP2 dispersion into two, one strong and one weak, curves. Therefore, the SPP-MP2 interaction will cause the relatively large frequency shift of the original MP2 mode. On the other hand, the anti-crossing effect is not observed in the coupling between SPP and MP3 modes: as in Fig. 3 for $\theta_x = 0°$, the MP3 is superposed with the SPP, resulting in a single reflectance dip with a wider full width at half minimum.

4.2. Localized Surface Plasmon

The localized surface plasmon is attributed to the collective oscillation of free electrons confined to subwavelength-sized conductors, such as metal nanoparticle, nanowire and nanodisc

#149604 - $15.00 USD Received 21 Jun 2011; revised 30 Jul 2011; accepted 3 Aug 2011; published 10 Aug 2011

[34]. The evanescent waves associated with the LSP result from the light scattering by the sub-wavelength object. For the structure under investigation, each square cross-sectional nanoslab can support the LSP since its size is much smaller than the light wavelength. Similar to the MP, the resonance frequency of the LSP mainly depends on the geometry of the structure and the intrinsic material property. Therefore, in principle the LSP excitation frequency should be independent of the incidence angle and the polarization state of the incident light. In Figs. 3 and 6, the reflectance dips at 10000 cm^{-1} and 11600 cm^{-1} are due to the LSP excitation. Note that the LSP frequencies do not shift for different incidence angles except when the LSP mode is coupled with other resonance modes, such as at $\theta_x = 40^\circ$ for *p*-polarization. The origin of the small dip at 9500 cm^{-1} for *s*-polarization is not clear yet and needs to be further investigated.

In order to prove that the reflectance dips at 10000 cm^{-1} and 11600 cm^{-1} result from the LSP excitation, we have calculated the reflectance of the nanoslabs aligned on a free standing SiO_2 film having identical geometric parameters as the 2-D structure under investigation, except that there is no Ag substrate. As can be seen from Fig. 8, both structures have two reflectance dips at the same wavenumbers, i.e., at 10000 cm^{-1} and 11600 cm^{-1}. From the fact that the reflectance dips occur at the same wavenumbers without the Ag substrate, we can infer that this resonant behavior is strongly confined in the nanoslabs. Furthermore, since both magnetic polaritons and surface plasmon polaritons cannot be excited without the presence of Ag substrate, only possible mechanism of the reflectance dips for the freestanding SiO_2 layer with the nanoslabs should be owing to the excitation of LSP.

The LSP can also be coupled with the SPP and the MP modes at a certain condition on the considered structure. As the SPP frequency varies with the incidence angle while the LSP and MP frequencies are nearly fixed, the SPP can be coupled with the LSP and MP modes to alter the reflectance spectrum in terms of the dip position as well as the dip value. For $\theta_x = 40^\circ$ in Fig. 3, for instance, the SPP mode interacts with the LSP2 and MP2 modes to shift the LSP2

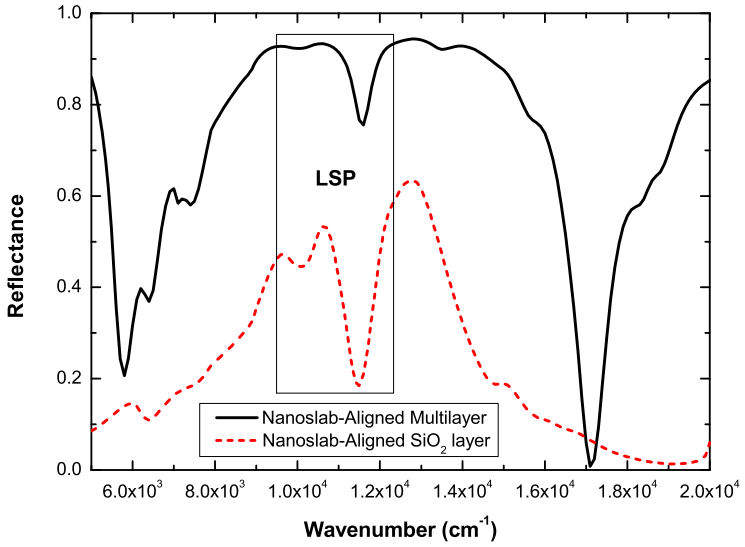

Fig. 8. Reflectance spectra of the nanoslab-aligned multilayer structure (solid line) and nanoslab-aligned freestanding SiO_2 film (dashed line) for the normal incidence.

#149604 - $15.00 USD Received 21 Jun 2011; revised 30 Jul 2011; accepted 3 Aug 2011; published 10 Aug 2011

frequency to 11200 cm^{-1} and the MP2 frequency to 13000 cm^{-1}. Since the SPP intensity is much stronger than the LSP2, the LSP2 is present as a shoulder near the SPP reflectance dip. Notice that Eq. (1) predicts the SPP frequency to be 12000 cm^{-1} for $\theta_x = 40^\circ$, which are close enough to be coupled with the LSP2 mode at 11600 cm^{-1} and the MP2 mode around 12600 cm^{-1}. The coupling between different modes results from the angle dependence of the SPP resonance. Hence the coupling effect cannot be observed in the reflectance spectrum for *s*-polarization, in which the SPP cannot be excited (refer to Fig 6).

For the considered 2-D nanoslab-aligned multilayer structure, we have identified the magnetic polariton, surface plasmon polariton, and localized surface plasmon modes in the wavenumber region between 5000 cm^{-1} and 20000 cm^{-1}. Calculation of the dispersion curves for each mode in 2-D configurations is computationally very expensive and challenging. The present work thus employed an alternative way of identifying each mode by examining the reflectance spectrum for different polarization and incidence angles and also by imaging the magnetic field distribution on the $x-y$ interface. In general, the MP can be distinguished from the SPP by observing the reflectance dip location while varying either the incidence angle or the grating period. As mentioned earlier, the resonance frequency of the MP should be nearly independent of the incidence angle and the grating period in contrast to that of the SPP. The LSP is also different from the SPP, such that the LSP is nearly independent of the incidence angle, the grating period, and the polarization state. In order to distinguish the LSP from the MP modes, one can calculate the reflectance of the freestanding nanoslab-aligned dielectric layer since the MP modes cannot be supported if no substrate exists.

5. Asymmetric nanoslab-aligned multilayer structure

Let us investigate the effect of the asymmetry of the nanoslab on the radiative properties. To this end, the rectangular nanoslab with $w_x = 250$ nm and $w_y = 300$ nm was considered instead of the square nanoslab. Figure 9 shows the normal reflectance of the rectangular nanoslab-aligned multilayer structure for *p*- and *s*-polarizations, along with the square nanoslab case (i.e., $w_x = w_y = w = 250$ nm) for comparison. When *p*-polarization is considered for the rectangular nanoslab, the LSP at 11600 cm^{-1} is shifted outside the wavenumber window under consideration while the resonance frequencies of the MP1 and MP3 modes are nearly unchanged. On the other hand, for *s*-polarization shown in Fig. 9(b), the LSP at 11600 cm^{-1} remains unchanged, but the MP1 and MP3 modes shift to the lower frequency. This could be understood as follows. The direction of MP resonance is defined as the direction along which the anti-nodes of the magnetic field are formed. As shown in Figs. 4 and 5, the direction of MP resonance is parallel to the electric field, i.e., *x*-direction for *p*-polarization. Therefore, the key parameter for the MP resonance frequency is the nanoslab length along the direction of the electric field. Since the rectangular nanoslab has the same length in the *x*-direction with the square nanoslab, i.e., $w_x = w = 250$ nm, the MP modes should occur nearly the same frequency for both square and rectangular nanoslab-aligned multilayer structure under the *p*-polarized incidence. On the other hand, Figs. 9(a) and 9(b) suggests that the LSP resonance frequency is very sensitive to the nanoslab length perpendicular to the direction of the electric field, i.e., w_y for $p-$polarization and w_x for $s-$polarization. This direction-dependence of the LSP excitation is counterintuitive, but can be qualitatively explained by considering the analogy with the LSP excitation of high-aspect-ratio nanomaterials, such as metallic nanorods. Previous studies revealed that metallic nanorods have two LSP resonances in low- and high-energy absorption bands, where the high-energy band LSP corresponds to the electron oscillations perpendicular to the major axis while the low-energy absorption band LSP results from the electron oscillations along the major axis [35]. Thus, LSP at 11600 cm^{-1} should correspond to the high-energy band, as electron oscillations are perpendicular to the major axis, or w_y for the rectangular nanoslab, for

#149604 - $15.00 USD Received 21 Jun 2011; revised 30 Jul 2011; accepted 3 Aug 2011; published 10 Aug 2011

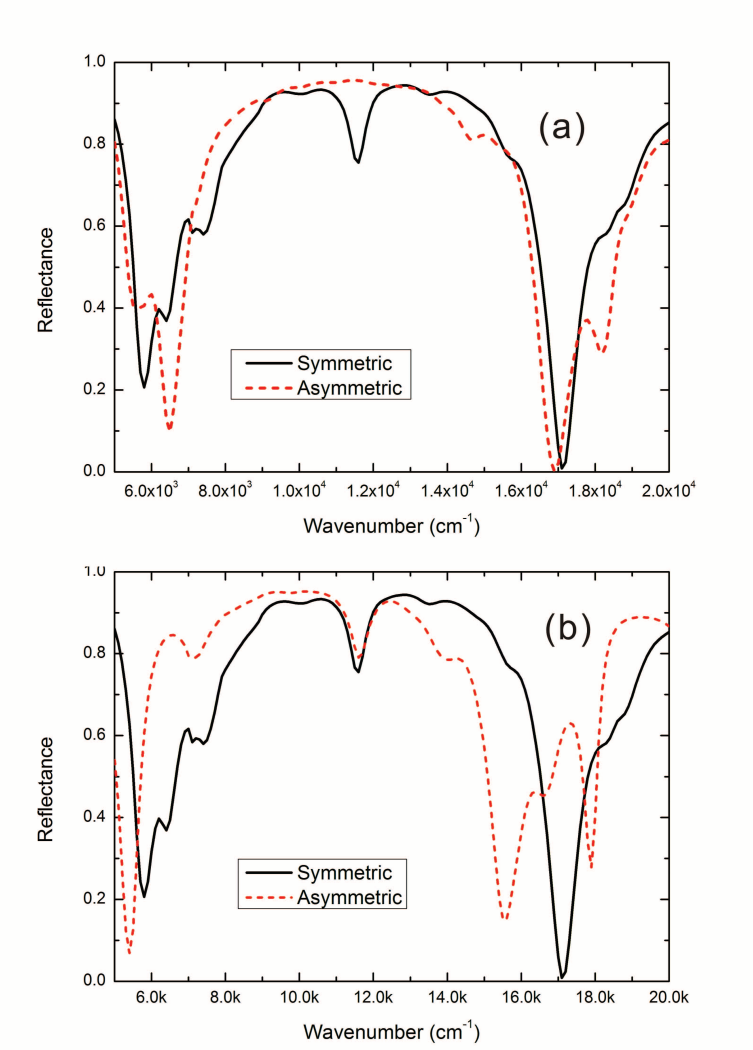

Fig. 9. Reflectance of the symmetric (solid line) and asymmetric (dashed line) nanoslab-aligned multilayer for the normal incidence under: (a) *p*-polarization and (b) *s*-polarization.

p−polarization: the increase of w_y will shift the high-band LSP frequency to a lower value [36]. Figure 9 clearly demonstrates that the nanoslab lengths into the *x*- and *y*-directions provide an additional degree of freedom to tailor the radiative properties of the nanoslab-aligned multilayer structure.

6. Concluding Remark

The present paper describes the theoretical investigation on the radiative properties of a 2-D multilayer structure that has a dielectric spacer between a metallic substrate and square cross-sectional nanoslabs. The 2-D rigorous coupled-wave analysis has been developed to calculate the spectral reflectance of the multilayer structure as well as the magnetic field distribution in the near field. It has been demonstrated that the nanoslab-aligned multilayer structure can sup-

#149604 - $15.00 USD Received 21 Jun 2011; revised 30 Jul 2011; accepted 3 Aug 2011; published 10 Aug 2011

port the plasmonic resonances, such as surface plasmon polariton and localized surface plasmon, as well as the magnetic polariton. The primary advantage of the 2-D nanoslab-aligned multilayer structure, when compared to the 1-D strip-aligned multilayer structure, is that the magnetic polariton for the 2-D structure is independent of the incidence angle and the polarization state of the incident light. The interactions between SPP, LSP, and MP modes have been observed to enhance the absorption of the incident light in certain conditions. Furthermore, the asymmetric geometry of the nanoslab can provide an additional degree of freedom to tailor the radiative properties of the considered structure. The results obtained in this study will facilitate the development of engineered nanostructures for real-world applications related with the renewable energy conversion, such as thermophotovoltaic and photovoltaic devices, where the tunability of the radiative properties independently of the incidence angle and/or the polarization state is important.

Acknowledgment

This work was mainly supported by the National Science Foundation (CBET-0966868 through PITT and CBET-1067441through URI). BJL thanks for the partial support from the startup program at KAIST, and KP also appreciates the partial support from the RI/Brown RI Consortium for Nanoscience and Nanotechnology.

#149604 - $15.00 USD Received 21 Jun 2011; revised 30 Jul 2011; accepted 3 Aug 2011; published 10 Aug 2011